COBEM 2023 27TH INTERNATIONAL CONGRESS OF MECHANICAL ENGENEERING

ABCM Brazilian Society of Mechanical Sciences and Engineering
27th ABCM International Congress of Mechanical Engineering
December 04-08, 2023, Florianópolis-SC, Brazil

COB-2023-1566
SLOT DIE COATING OF THIXOTROPIC LIQUIDS

Carlos E. Sanchez Perez
Danmer Maza
Paulo R. de Souza Mendes
Marcio S. Carvalho
Department of Mechanical Engineering, Pontifícia Universidade Católica do Rio de Janeiro
Rua Marquês de São Vicente, 225, 22451-900. Rio de Janeiro, Brazil
csanchez@lmmp.mec.puc-rio.br; danmer@lmmp.mec.puc-rio.br; pmendes@puc-rio.br; msc@puc-rio.br

Abstract. *Many particle suspensions behave as thixotropic-viscous materials and are present in different industrial processes, including coating applications. Specifically, the production of battery electrodes includes slot coating of thixotropic liquids. In most cases, the flow of slurries and other particle suspensions is described using a generalized Newtonian model that assumes the viscosity to be solely a function of the local deformation rate. However, the viscosity of thixotropic fluids is associated with their microstructuring level. The viscosity does not change instantaneously with the stress (or deformation rate). In the case of imposing constant stress (or shear rate), the microstructure evolves until reaching an equilibrium state, but this process takes time. In the particular case of slot coating, the liquid flows through regions where there are significant changes in the levels of stress. Assuming that the viscosity at each point of the flow is the steady-state viscosity described by a generalized Newtonian model may lead to an inaccurate flow description and predictions of the stable operating conditions. The flow of a thixotropic-viscous liquid through a slot coater is analyzed here using two rheological models: the generalized Newtonian model (GNM) and a generalized Newtonian thixotropic model (GNTM) that considers the liquid's time-dependent response. The resulting set of fully coupled, non-linear equations is solved by the Galerkin and SUPG Finite Element Method. The results show that the use of a simple GNM to describe thixotropic viscous materials, such as some particle suspensions, can lead to very large errors in the predicted flow behavior. Furthermore, time-independent generalized Newtonian models are not able to predict flow phenomena like hysteresis, which could provoke unstable flows. These inaccuracies highlight the need for a more complete model that considers the time-dependency of the flowing liquid within a certain range of flow parameters.*

Keywords: *slot coating, thixotropy, generalized Newtonian model, particle suspensions, fluidity*

1. INTRODUCTION

There are interesting and important fluids in industry and other human activities, like coating applications, that cannot be described by simple models which relate viscosity with just rate of strain or shear stress. Examples of complex liquids with these features are particle suspensions. Despite the Newtonian nature of the solvent, the addition of solid-dispersed phase introduces different non-Newtonian behaviors (Mueller *et al.*, 2010) like time-dependent behaviors. The viscosity of many particle suspensions decreases with time, while a constant stress is applied to a sample that has been previously at rest, and the subsequent recovery of viscosity in time as the flow ceases (Mewis and Wagner, 2009). This mechanical behavior is called thixotropy, which also implies "fluid memory" which is associated with shear history (Mewis and Wagner, 2009). Thixotropy is usually associated with reversible microscopic arrangements of the particles in a suspension (Mewis and Wagner, 2009; de Souza Mendes *et al.*, 2018).

Coating is an industrial process where one or more liquid layers are deposited on a surface; then they are dried or cured to form solid films to serve a particular purpose (Kisler and Schweizer, 1997). This technique is used in the manufacturing of many products, including battery production. A sketch of this flow is shown in Fig. 1. The suspension is pumped and delivered into a coating die. Then, the coating liquid is applied onto a solid surface (substrate) through a narrow slot. As a result, the suspension fills the gap between the adjacent die lip and the substrate. The area covered by the suspension in the gap, bounded by the upstream and downstream gas-liquid interfaces, is called *coating bead*.

To maintain a stable coating bead and/or produce a thin deposited film without defects, the upstream gas pressure is usually below ambient pressure (P_{vac} shown in Fig. 1) by employing a vacuum chamber (Beguin (1954) as cited by Rebouças *et al.* (2018)). However, in some specific processes where thick film is produced, vacuum pressure is not necessary (Yoon *et al.*, 2022).

Slot coating belongs to a class of coating methods known as *pre-metered coating*. The thickness of the coated liquid layer (h) is set by the flow rate (q) fed into the die and the speed of the moving substrate (V_w), i.e. $h = q/V_w$. Therefore, it is independent of other process variables (Carvalho and Kheshgi, 2000). Thus pre-metered methods are ideal for high precision coating. However, the uniformity of the deposited layer and therefore the quality of the product depend on other

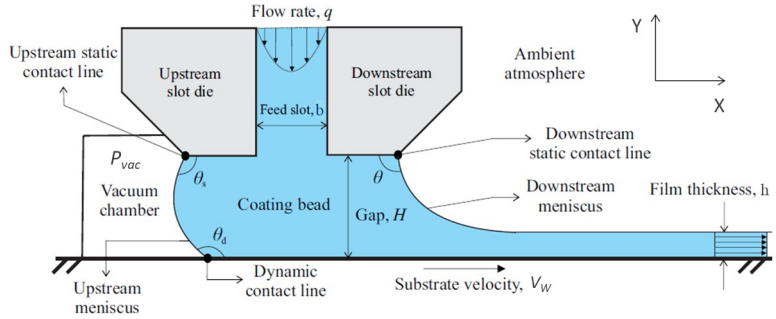

Figure 1. Sketch of the slot coating process (Adapted from Siqueira and Carvalho (2019))

parameters, such as liquid viscosity and its rheology, vacuum pressure applied, superficial tension, coating gap, slot die configuration, etc (Ding *et al.*, 2016). As a result, there are limits in operating conditions of slot coating. Working beyond these limits leads to a coating product with defects.

The most common defects related to the operating limits of slot coating are: air entrainment, dripping and rivulets (Ding *et al.*, 2016). One of these operating limits defines the minimum coated film thickness achievable (h_{min}), which is also called *low flow limit*. Beyond this limit, the downstream free surface penetrates into the coating bead. This phenomenon occurs since this air-liquid interface is very curved, so it becomes unstable. As a result, it is registered a periodic variation in the transverse section in the film thickness deposited onto the solid surface. Eventually, the non-uniformity leads to alternating stripes of coated and uncoated layers, called *rivulets* (Ding *et al.*, 2016). The other two operating limits are defined by the vacuum pressure applied. If P_{vac} is too low, for a given film thickness (h) , the downstream meniscus invades the coating bead and rivulets could be formed in the coated layer. In the case of a too high P_{vac}, the upstream meniscus invades the vacuum chamber. This phenomenon is called dripping, at which the pre-metered characteristic of slot coating is lost.

The region bounded by the operating limits mentioned above, at which a coating product is delivered with acceptable quality, is defined as *coating window*. Figure 2 offers a sketch of typical coating window for Newtonian fluids. Defining the limits of these windows is a difficult task, even for Newtonian fluids. Nevertheless, there is extensive literature about coating windows for Newtonian liquids. For instance, Higgins and Scriven (1980) analytically defined the vacuum pressure and film thickness operating ranges. The work by Higgins and Scriven (1980) presents the visco-capillary model used as a reference for coating of Newtonian liquids.

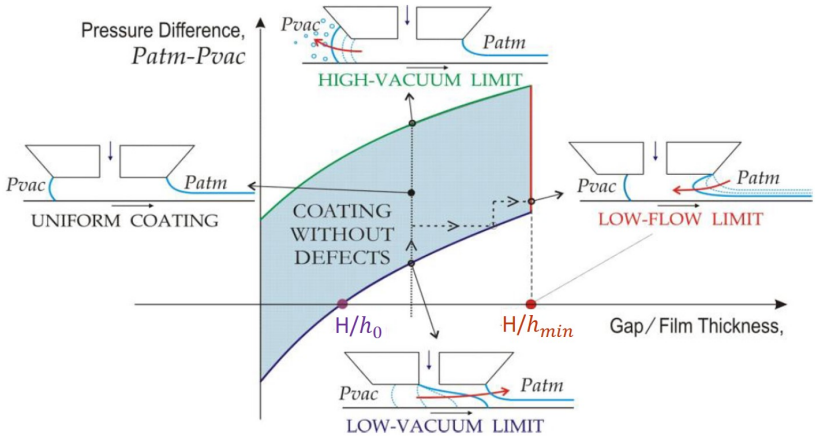

Figure 2. Sketch of a typical coating window for Newtonian fluids (Adapted from Valdez (2013))

In the case of non-Newtonian coating, the literature is much more restricted. However, there are various works where the rheology of the coating liquid is considered. Many of this works have incorporated generalized Newtonian equations into the visco-capillary method. For instance, Tsuda (2010) uses the Power-law model and the pressure field equation proposed by Higgins and Scriven (1980). The results show variations on the operability parameters compared to the Newtonian models. Siqueira and Carvalho (2019) determined the operability limits for non-colloidal particle suspensions.

The inclusion of time-dependence response adds much more complexity and computing costs in modeling a complex thixotropic flow. On the other hand, modeling complex flows of thixotropic materials using models that neglect time-dependent effects may lead to inaccurate predictions (Link *et al.*, 2015). In the particular case of slot coating of particle suspensions, the inaccurate prediction of the process limits may lead to the prediction of process conditions that will yield

products with defects.

The main goal of this work was to evaluate the effects of thixotropy on flow pattern and process limits. To describe the thixotropic flow was used the rheological model proposed by de Souza Mendes *et al.* (2018). In this thixotropic model, the traditional evolution equation as a function of the parameter λ, which describes the microstructuring level of the liquid, was replaced by a novel evolution equation as a function of fluidity (ϕ_v). The latter parameter is just the reciprocal of viscosity (as defined by Fredrickson (1970)). A time-independent model was used as a base case to evaluate the time-dependent effects. It is also important to note that ideal thixotropy is only considered in the present work. In other words, it was selected an inelastic thixotropic liquid as a reference.

2. MATHEMATICAL FORMULATION AND METHODOLOGY

We consider a small-scale, steady-state flow of a non-Newtonian liquid that exhibits shear-thinning and thixotropy. Gravitational forces are neglected. The flow is described by incompressible mass and momentum conservation equations:

$$\nabla \cdot \boldsymbol{u} = 0 \tag{1}$$

and

$$\rho \boldsymbol{u} \cdot \nabla \boldsymbol{u} = \nabla \cdot \boldsymbol{T} \tag{2}$$

where $\boldsymbol{u}$ is the velocity vector, ρ is the liquid density, $\boldsymbol{T}$ is the stress tensor. The stress tensor is split as $\boldsymbol{T} = -p\boldsymbol{I} + \boldsymbol{\tau}$, where p is the pressure field, $\boldsymbol{I}$ is the identity tensor, and $\boldsymbol{\tau}$ is the extra stress tensor. The latter obeys Newton's law of viscosity, $\boldsymbol{\tau} = \eta(\nabla \boldsymbol{u} + \nabla \boldsymbol{u}^T)$, where η is the local viscosity of the liquid.

2.1 Rheological models

Two different rheological models are considered in the analysis. One model is time-independent while the second considers the time-dependent effects. Since it is not considered elastic features, both models belong to the category of *generalized Newtonian models* and they obey the Newton's law of viscosity. However, for simplicity the time-independent model is referred here as the *generalized Newtonian model (GNM)* while the second as *thixotropic model or GNTM*.

GNM neglects fluid time-dependent effects and assumes that the viscosity at each point is just a function of the local deformation rate $\dot{\gamma}$.

$$\eta_v = \eta_v(\dot{\gamma}) \tag{3}$$

The function $\eta_v(\dot{\gamma})$ is obtained experimentally and it is generally referred to as the liquid flow curve. As liquid of reference was used a Laponite suspension, described in detail by de Souza Mendes *et al.* (2018). The yield stress of the Laponite suspension was low and we set its value to zero to ease the numerical convergence. Furthermore, ϕ_0 was fixed at 10^{-3} $(Pa.s)^{-1}$. The flow curve and the corresponding variation of ϕ^*_{eq} with the local stress is presented in Fig. 3.

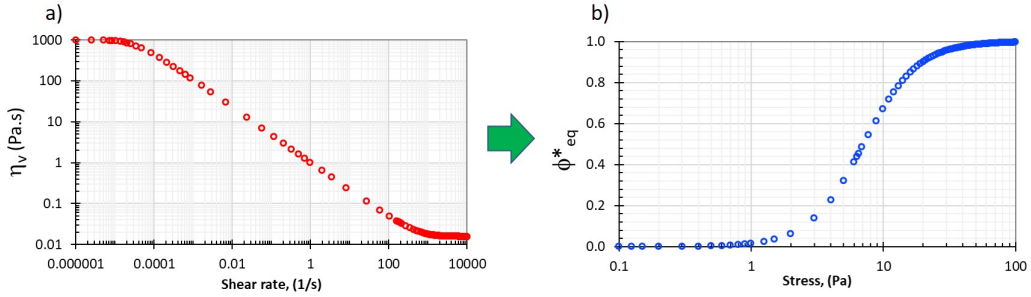

Figure 3. a) Steady state viscosity as function of the shear rate; b) Normalized equilibrium fluidity as function of shear stress for a hypothetical suspension with $\sigma_y = 0\ Pa$ and $\phi_0 = 10^{-3}(Pa.s)^{-1}$

The fluidity equation, ϕ^*_{eq}, shown in Fig. 3, is given by:

$$\phi^*_{eq}(\sigma) = \frac{\frac{1}{\sigma}\left[\frac{\sigma}{K}\right]^{1/n}}{(\phi_\infty - \phi_0) + \frac{1}{\sigma}\left[\frac{\sigma}{K}\right]^{1/n}}, \tag{4}$$

where for the Laponite suspension used as example by de Souza Mendes *et al.* (2018), $K = 1\ Pa.s^n$, $n = 0.32$, $\phi_\infty = 64.1(Pa.s)^{-1}$, and $\phi_0 = 10^{-3}(Pa.s)^{-1}$.

Having in mind the concept of fluidity (i.e. reciprocal of viscosity) and the definition of normalized fluidity, the steady-state viscosity as a function of the local stress is written as:

$$\eta_v(\sigma) = 1/\phi_v = [\phi^*_{eq}(\sigma)(\phi_\infty - \phi_0) + \phi_0]^{-1} \tag{5}$$

The generalized Newtonian thixotropic model takes into account the fluid time-dependent response, and is referred to as the *thixotropic model* or *GNTM* . The mechanical response of the liquid is described by the model proposed by de Souza Mendes *et al.* (2018). The main advantage of this model, when compared to existing phenomenological models for thixotropic materials, is that the evolution equation that describes the microscopic state only involves material functions that are directly measurable by means of standard rheological tests. The evolution equation for fluidity is written as Eq. (6). The function that describes the rate of change of fluidity $F(\phi^*_v, \phi^*_{eq}(\sigma))$ is written using two different functional forms, depending whether the structure is being broken or recovered, as shown in Eq. (7).

$$\boldsymbol{v} \cdot \boldsymbol{\nabla}\phi^*_v = F(\phi^*_v, \phi^*_{eq}(\sigma)) \,, \tag{6}$$

$$F(\phi^*_v, \phi^*_{eq}(\sigma)) = \begin{cases} f_b = \frac{s}{t_a \phi^*_{eq}(\sigma)} (\phi^*_{eq} - \phi^*_v)^{\frac{s+1}{s}} {\phi^*_v}^{\frac{s-1}{s}}, & 0 < \phi^*_v \leq \phi^*_{eq} \\ f_c = -\frac{(\phi^*_v - \phi^*_{eq})}{t_c}, & \phi^*_{eq} < \phi^*_v \leq 1 \end{cases} \tag{7}$$

where, the avalanche time t_a and the exponent s are a function of the equilibrium fluidity.

$$t_a(\phi^*_{eq}) = 59.2 \frac{(1 - \phi^*_{eq})^{1.1}}{{\phi^*_{eq}}^{0.4}}, \tag{8}$$

$$s = \frac{8}{\exp(\phi^*_{eq}/0.09) - 1} + 1.2. \tag{9}$$

The functional form for $\phi^*_{eq} < \phi^*_v \leq 1$ represents the structure buildup dynamics. For the Laponite suspension, the construction time is $t_c = 663$ s.

It is important to mention that the functional forms presented in Eq. (7) were proposed based on the rheological response of a Laponite suspension. The functional form $F(\phi^*_v, \phi^*_{eq}(\sigma))$ will change with the fluid rheological response.

2.2 Flow geometry and boundary conditions

We investigated the flow in slot coating process. At the feed slot, the flow kinematics show regions of fully developed flow, at which the fluidity is in equilibrium along every streamline. However, as the liquid enters into the coating bead, the initial equilibrium is perturbed. A liquid particle goes through different regions of the flow, at which the Lagrangian variation of the stress is complex. Since the thixotropic model takes into account the time response to stress changes, modeling the liquid behavior as a thixotropic fluid may lead to very different flow fields from those computed with a simple GNM.

A sketch of the geometry of the problem is shown in Fig. 4. It is possible to visualize how the domain was discretized and what boundary conditions were used. The boundary conditions are the same ones used by Rebouças *et al.* (2018); Siqueira and Carvalho (2019). The boundary conditions that were adopted are the following:

1. *Moving substrate: No-slip and no-penetration conditions are used.*

   $$u = V_w \quad ; \qquad v = 0. \tag{10}$$

   V_w is the substrate velocity.

2. *Outflow: Fully developed flow.*

   $$\hat{\boldsymbol{n}} \cdot \nabla \boldsymbol{u} = 0. \tag{11}$$

   and $p = p_{amb}$, where p_{amb} is the ambient pressure and its manometric value is taken as 0.

3. *Free surfaces:* The shear stress vanishes. Furthermore, there is a force balance due to the external pressure and the capillary pressure originated by the curvature of the free surface.

   $$\hat{\boldsymbol{n}} \cdot \boldsymbol{u} = 0 \quad ; \quad \hat{\boldsymbol{n}} \cdot \boldsymbol{T} = \frac{1}{Ca} \frac{d\boldsymbol{t}}{ds_c} - \hat{\boldsymbol{n}} p_g. \tag{12}$$

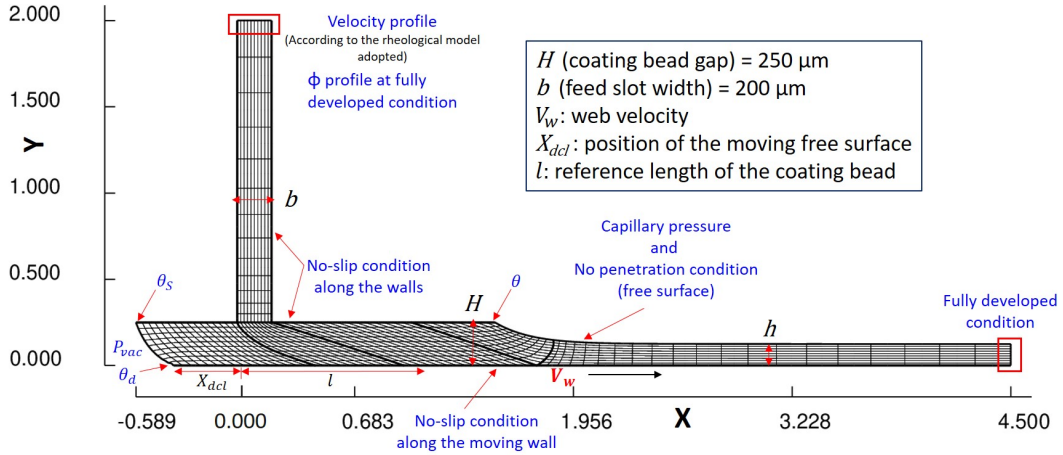

Figure 4. Sketch of the slot coater device simulated, including dimensions and boundary conditions.

t and ***n*** are the unit tangent and unit normal vector along the free surface, while s is the arc length of the free surface and Ca is the capillary number. In addition, P_g is the external gas pressure.

It is important to notice that $P_g = P_{amb}$ at the downstream free surface, while $P_g = P_{vac}$ at the upstream free surface. P_{vac} is the pressure imposed at the vacuum chamber, which is usually lower than P_{amb}. For given values of V_w and h (film thickness), the value of P_{vac} defines the position of the dynamic free surface ($\boldsymbol{X}_{dcl}$).

4. *Static contact line: Pinned at the corner of the die lip.*

$$\boldsymbol{X}_{scl} = \boldsymbol{X}_{corner}. \tag{13}$$

5. *At the solid walls: No-slip and no-penetration conditions are employed.*

6. *Inflow: Fully developed flow. It is necessary to impose a coherent velocity profile at the feed slot inlet. In fact, this velocity profile should correspond to a fully developed flow and rheologically coherent to Eq. (5).*

2.3 Dimensionless numbers

The velocity of the moving plate (V_w) and the coating gap (H) are used as characteristic velocity and length. The flow is governed by the following dimensionless parameters:

1. Reynolds number, which represents the ratio of inertial and viscous forces, defined as:

$$Re \equiv \rho V_w H/\eta_{ref},$$

where, η_{ref} is a reference viscosity. The maximum value of Re is about 0.127.

2. Capillary number, which represents the ratio of viscous and interfacial forces, defined as:

$$Ca \equiv \eta_{ref} V_w/\Gamma_s,$$

where, Γ_s is the surface tension of the liquid and it was set in 60 mN/m, according to typical values in particle suspensions.

3. Gap-over-thickness ratio, defined as:

$$G = H/h,$$

where, h is the film thickness.

4. Thixotropy number, which represents the ratio of the construction time to the liquid residence time in the coating bead (or part of it), defined as:

$$\Lambda = V_w t_c/l.$$

This is the inverse of the Mutation number Mu, defined by Mours and Winter (1994), and discussed in detail by Jamali and McKinley (2022). In the calculations, it was used l = 1 mm. This parameter is the reference length of the coating bead from the beginning of the feed slot, as shown in Fig. 4.

All results reported here were obtained considering V_w = 25 mm/s.

2.4 Numerical formulation

Numerical solutions were obtained via finite element approximations of the mass and momentum conservation equations, and fluidity evolution equation (when using the thixotropic model) with the appropriate boundary conditions. For slot coating results, it is also necessary to determine the position of the free surfaces. This is done by a mapping between the unknown physical domain and a known computational/reference domain according to the elliptic mesh generation method. The resulting differential equation is also part of the set of equations solved by the finite element method.

The independent variables of the problem, i.e. velocity, pressure, fluidity (for the thixotropic model) fields, and mesh position are written as a linear combination of a finite number of basis functions. Lagrangian biquadratic functions were used to represent the velocity field and mesh position, linear discontinuous functions were used for the pressure field and Lagrangian biquadratic for the fluidity field. Galerkin's weighting functions are used in the residual equations of mass and momentum conservation, and mesh equation, whereas the stabilized Streamline-Upwind Petrov-Galerkin formulation is applied in fluidity transport equation. The upwinding parameter was defined as the characteristic size of the smallest element in the computational mesh.

The flow domain was divided into quadrangular finite elements using a computational mesh with 760 elements and 3225 nodes. The G/SUPG FEM formulation reduces the fully coupled, non-linear model to a large, sparse set of coupled, non-linear algebraic equations with 18,405 degrees of freedom for the thixotropic model and 15,180 degrees of freedom for the time-independent model. The resulting global set of non-linear equations was solved by Newton's Method with a numerical Jacobian matrix calculated using a second-order central difference scheme. The tolerance on the L2-norm of the Newton update and of the global residual vector were both set to 10^{-6}. At each iteration of Newton's Method, the linear system was solved with a frontal solver based on the LU factorization scheme.

3. RESULTS

The results presented here compares the operability limits in the plane of vacuum pressure and gap-over-thickness ratio predicted by both rheological models at the web velocity V_w equal 25 mm/s. The corresponding capillary and thixotropy number are Ca = 0.021 and $\Lambda = 1.66\times10^4$. The operability limits predicted by the time-independent model are presented in Fig. 5a. The high vacuum limit (red squares) is characterized by the conditions at which the dynamic contact line position is equal the length of the upstream die lip, i.e. X_{dcl} = -1.5 mm, whereas the low vacuum limit (blue triangles) is characterized by the conditions at which the dynamic contact line reaches the feed slot, i.e. X_{dcl} = 0. The low flow limit (black circles) is marked by the invasion of the downstream meniscus, characterized by a low contact angle between the downstream meniscus and the downstream die lip. P_{vac} is referred here to the gauge vacuum pressure.

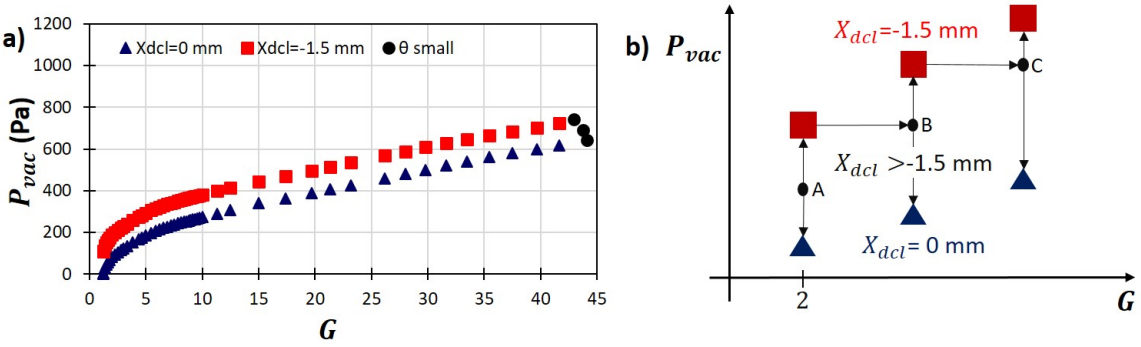

Figure 5. a) Slot coating operating window obtained from the GNM. b) Sketch of the procedure carried out to obtain the slot coating operating windows.

The high and low vacuum limit curves were obtained from the numerical solution in the following way, as sketched in Fig. 5b: First a stable solution at a G=2 was obtained with a value of vacuum pressure such that the dynamic contact line position was in the middle of the upstream die lip, i.e. $-1.5\ mm < X_{dcl} < 0\ mm$. This flow state is labeled A in Fig. 5b. The value of vacuum pressure was slowly decreased, with all the other parameters fixed, until X_{dcl} = 0 mm. This is the first point of the low vacuum limit curve. From flow state A, the value of the vacuum pressure was also slowly increased until X_{dcl} = -1.5 mm, which defines the first point of the high vacuum limit curve. From the high vacuum limit state, the film thickness was slightly decreased, which corresponds to a small increase in the value of gap-over-thickness ratio G. As the flow rate is reduced, the dynamic contact line moves downstream, and X_{dcl} > -1.5 mm. This flow state is labeled B in Fig. 5b. From flow state B, with a higher value of G, the vacuum pressure is again decreased and increased until X_{dcl} = 0 mm and X_{dcl} = -1.5 mm, respectively. The procedure is repeated until numerical solutions of the differential equations could not be obtained. Figure 6 presents the flow at the onset of low and high vacuum limit at G = 10. The low and high vacuum pressures were P_{vac} = 273.2 Pa and P_{vac} = 381.2 Pa, respectively.

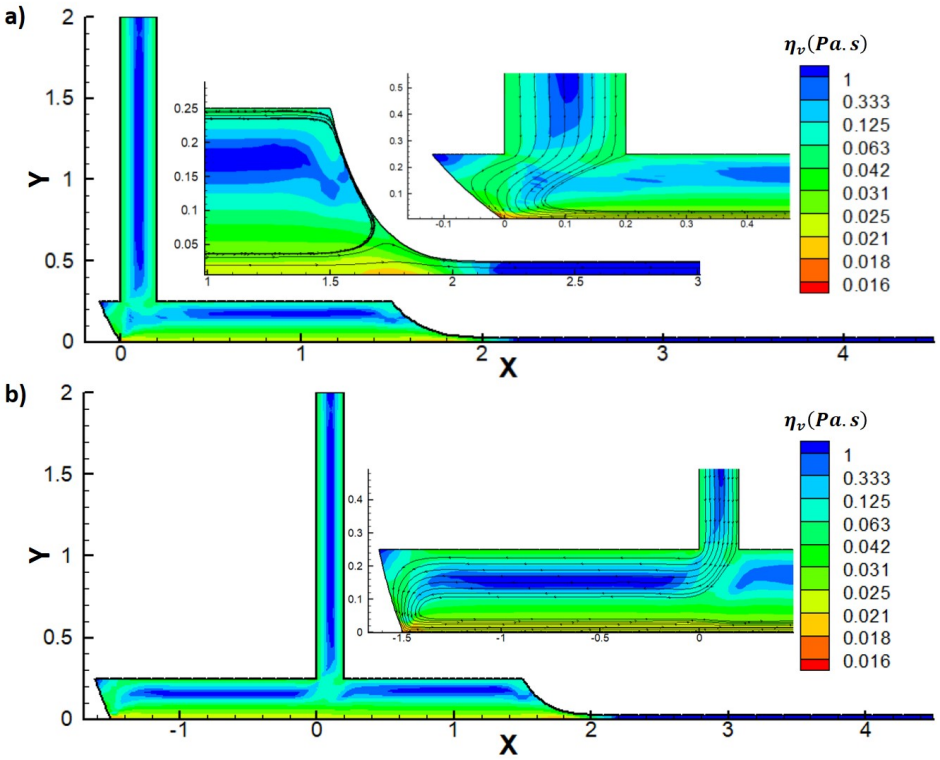

Figure 6. Viscosity fields according to the GNM for G=10, at a) X_{dcl}=0 mm and b) X_{dcl}=-1.5 mm.

There is a value of gap-over-thickness ratio above which the downstream meniscus invades the coating bead, which marks the onset of the low flow limit (black circles in Fig. 5a). At the conditions considered in this example, the low flow limit occurs at $G \approx 43$. The minimum thickness that can be coated is close to $h \approx H$ / 43. Figure 7 illustrates the flow configuration at the onset of low flow limit.

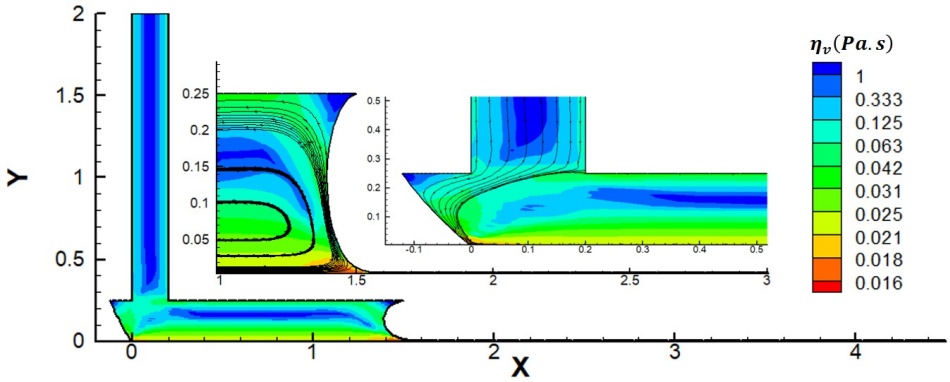

Figure 7. Viscosity field according to the GNM for G=43.3 at X_{dcl}=0 mm.

From flow state A, the procedure was repeated by now lowering the gap-over-thickness G to extend the high and low vacuum limit curves to lower values of G until the later crosses the horizontal axis, which marks the maximum value of G (or minimum value of the film thickness) possible when there is no vacuum pressure. For the time-independent model used, this value was G_0 = 1.23, considering a coating gap of 100 μm, the minimum thickness that can be coated without a vacuum box is $h \approx 81$ μm. At each value of G, there is a small range of vacuum pressure at which the contact line is located on the upstream die lip and the flow is stable. The level of vacuum pressure needed rises as the film thickness becomes smaller.

The operability limits predicted when using the thixotropic model is presented in Fig. 8. First, the high and low vacuum limit curves predicted when using the thixotropic model were obtained following the same procedure described before and sketched in Fig. 5b. The predicted maximum gap-over-thickness without vacuum was G_0 = 1.18. Considering a coating gap of 100 μm, if a vacuum box is not used in the process, the minimum thickness that can be coated is $h \approx$ 84.7 μm.

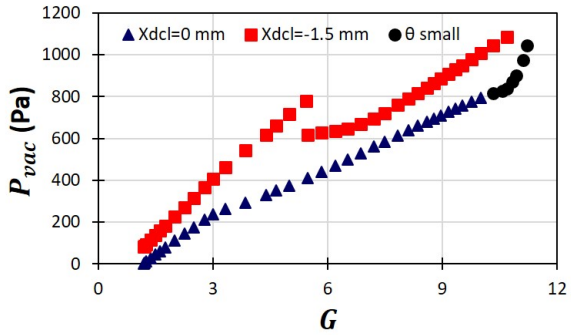

Figure 8. Slot coating operating window obtained from the thixotropic model.

However, at approximately $G \approx 5.5$, the procedure fails, and a solution cannot be obtained. The sequence of flow states that leads to the computation of the onset of process limits was changed and it was possible to construct the low vacuum limit curve continuously up to $G \approx 10$. From each flow state at the low vacuum limit and different values of gap-over-thickness ratio above $G \approx 5.5$, vacuum pressure was increased until X_{dcl} = -1.5 mm. The results presented in Fig. 8 show an interesting phenomenon: The computed high vacuum limit curve is not continuous. The two branches of the curve were obtained using different continuation strategies of flow states until reaching the desired condition. Two different flow states were obtained at the same flow conditions, which indicates a hysteresis in the dynamics of the system. In practice, this hysteretic behavior may lead to oscillation between the different stable flow states. Figure 9 presents the two flow states computed at G = 5.45, with X_{dcl} = -1.5 mm. The first one, Fig. 9a, belongs to the low G branch of the high vacuum limit curve and P_{vac} = 778 Pa; and the second one, Fig. 9b, to the high G branch of the curve with P_{vac} = 618 Pa. The figure presents the viscosity field and the streamlines near the exit of the feed slot. The main difference between the solutions is the flow pattern near the feed slot and under the upstream die lip. The higher vacuum pressure solution presented in Fig. 9a shows a complex recirculation pattern, with two saddle points and three recirculation centers. Part of the liquid coming out of the feed slot flows upstream, filling the upstream part of the coating bead, and part of the pumped volume flows directly downstream under the downstream die lip. The lower vacuum pressure solution presented in Fig. 9b presents a much simpler flow pattern. The recirculation under the upstream and downstream die lips are merged and all the liquid coming out of the feed slot flows upstream around the vortex before flowing downstream.

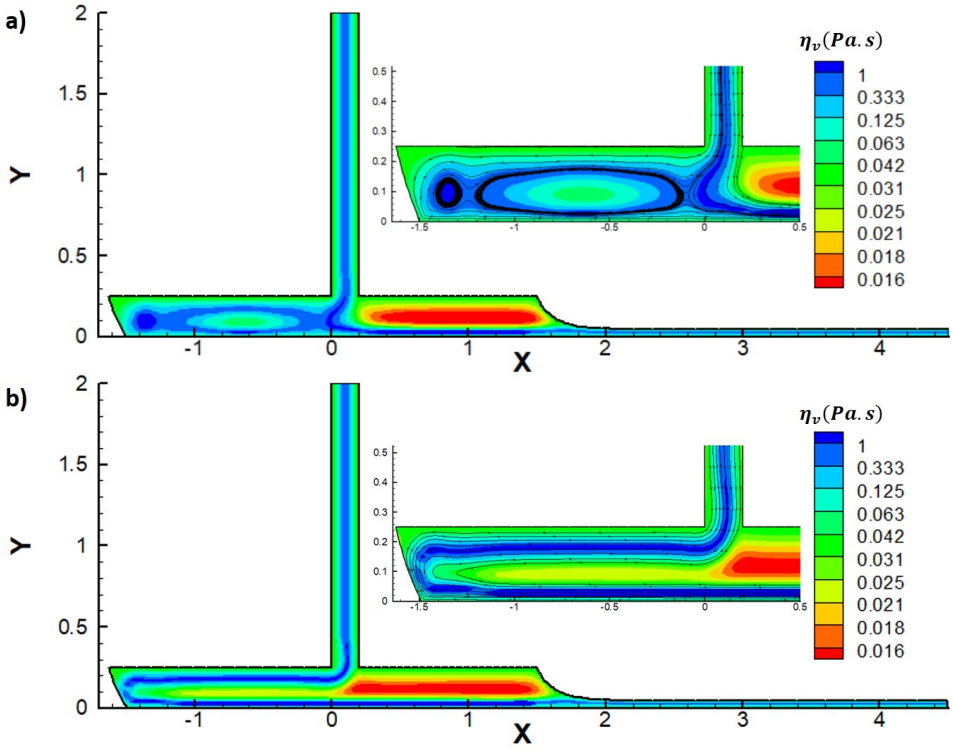

Figure 9. Hysteresis phenomenon for G=5.45 and X_{dcl}=-1.5 mm: a) P_{vac} = 778 Pa and b) P_{vac} = 618 Pa.

A simple comparison between the operability limits presented in Fig.5a and 8 shows that the range of operating

parameters, e.g. gap-over-thickness ratio G and vacuum pressure P_{vac}, that leads to stable flow in the coating bead is remarkably different. The range of vacuum pressure required to stabilize the upstream meniscus predicted by the thixotropic model is much higher than that predicted by the GNM. Figure 10 presents the flow states computed using both rheological models at the onset of the low vacuum pressure limit, i.e. X_{dcl} = 0, V_w = 25mm/s and G = 10. The necessary vacuum pressure when using the time-independent model is P_{vac} = 273.2 Pa, whereas it is P_{vac} = 795 Pa for the thixotropic model. The figure shows the computed viscosity field and the streamline pattern near the downstream meniscus and the exit of the feed slot. The viscosity near the upstream meniscus predicted by the thixotropic model is much higher than that predicted by the time-independent model. In the later, the viscosity is only a function of the local shear rate. Since the deformation rate under the die lip and close to the dynamic contact line are very high, the liquid viscosity is low in that region. With the thixotropic model, the liquid does not have enough time to change its microstructure and lower its viscosity in response to a high stress region, leading to a higher viscosity fluid near the upstream meniscus. Therefore, a higher vacuum pressure is required to push the upstream free surface upstream.

Another important difference between the two flow states is the configuration of the downstream free surface. The meniscus curvature in the time-independent model prediction is much smaller than that predicted by the thixotropic model. This can be explained also by comparing the viscosity field of both flows. It is important to remember that the downstream meniscus curvature creates the necessary adverse pressure gradient when the flow rate is low (thin coated film and high G). The more curved is the meniscus, the stronger adverse pressure gradient is formed. The deformation rate in the film formation region, e.g. 1.5 mm < X < 2 mm, is high due to the strong liquid acceleration. This leads to a low viscosity region in the time-independent flow. In the thixotropic flow, the viscosity is high in this region; the liquid does not have enough time to respond to the high stress in that region. Therefore, the necessary adverse pressure gradient in the thixotropic flow is higher than that required in the time-independent flow, which explains the higher curvature of the downstream free surface. Because of the high viscosity region near the web in the thixotropic solution, a higher adverse pressure gradient is necessary to meter the flow.

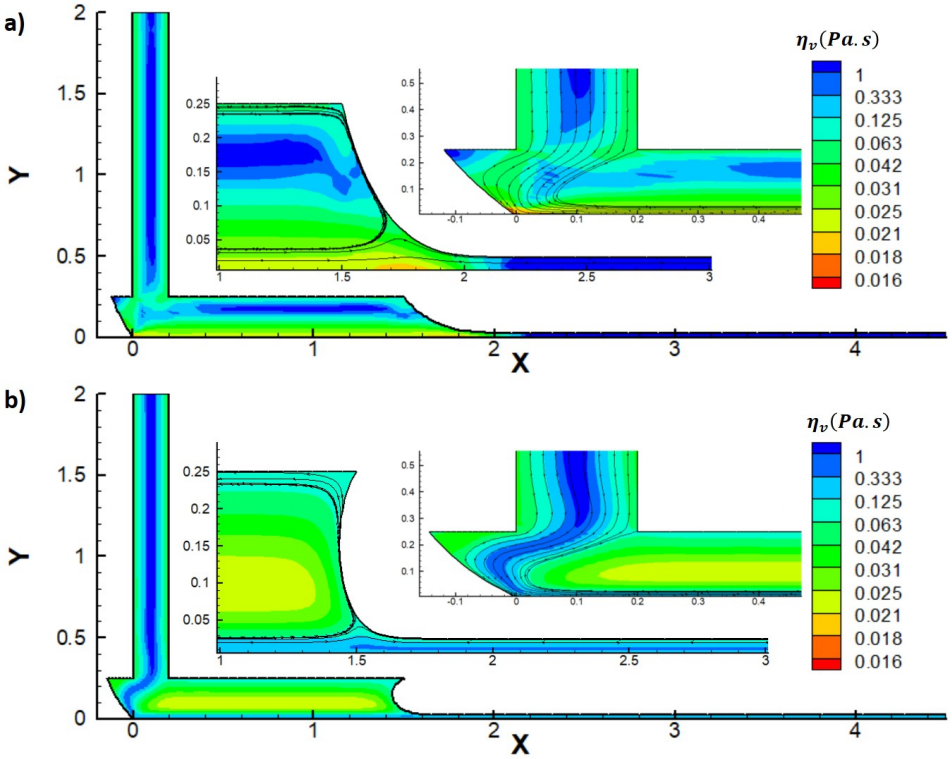

Figure 10. Viscosity fields for G=10 at X_{dcl}= 0 mm, according to: a) GNM and b) thixotropic model.

As discussed before, the configuration of the downstream meniscus has a strong effect on the onset of the low flow limit. The higher curvature of the downstream free surface observed in the thixotropic solution implies that the low flow limit occurs at lower values of the gap-over-thickness ratio, with implies that the minimum thickness that can be coated predicted with the thixotropic model is much larger than that predicted when time-dependent effects are neglected. The onset of the low flow limit predicted by the time-independent model is approximately G = 43.3, whereas the value predicted by the thixotropic model is close to G = 10.3. Considering a coating gap of 100 μm, a model that does not take into account the liquid time-dependent response predicts that the minimum thickness that can be coated at the conditions explored here is $h \approx 2.3$ μm and would require a vacuum pressure of $P_{vac} \approx 650$ Pa. When time-dependent effects are

considered in the model, the predicted minimum thickness that can be coated is $h \approx 9.3$ μm and would require a vacuum pressure of $P_{vac} \approx 950$ Pa.

4. CONCLUSIONS

In the present work, the effects of thixotropy on flow pattern and process limits were analyzed. The solutions obtained with the time-independent model were used as a base case to evaluate the time-dependent effects. All results were obtained using the thixotropic model and the rheological data of a laponite suspension obtained by de Souza Mendes *et al.* (2018). As time-independent model, referred as GNM, was used the flow curve of the thixotropic model proposed by de Souza Mendes *et al.* (2018)

For the Laponite suspension, used as example, the results reveal that modeling slot coating flow of inelastic liquids that exhibit time-dependent behavior with a time-independent model can lead to very inaccurate predictions of the operability window of the process. Moreover, the solutions obtained with the thixotropic model show hysteretic behavior, which a simple time-independent model is not able to predict. This behavior implies two different solutions at the same flow parameters, which may lead to strong oscillation of the flow.

5. ACKNOWLEDGEMENTS

The authors acknowledge CAPES and CNPQ for financial support.

6. REFERENCES

Carvalho, M.S. and Kheshgi, H.S., 2000. "Low-flow limit in slot coating: Theory and experiments". *AIChE Journal*, Vol. 46, No. 10, pp. 1907–1917.

de Souza Mendes, P.R., Abedi, B. and Thompson, R.L., 2018. "Constructing a thixotropy model from rheological experiments". *Journal of Non-Newtonian Fluid Mechanics*, Vol. 261, pp. 1–8.

Ding, X., Liu, J. and Harris, T.A.L., 2016. "A review of the operating limits in slot die coating processes". *AIChE Journal*, Vol. 62, No. 7, pp. 2508–2524.

Fredrickson, A.G., 1970. "A model for the thixotropy of suspensions". *AIChE Journal*, Vol. 16, No. 3, pp. 436–441.

Higgins, B. and Scriven, L., 1980. "Capillary pressure and viscous pressure drop set bounds on coating bead operability". *Chemical Engineering Science*, Vol. 35, No. 3, pp. 673–682.

Jamali, S. and McKinley, G.H., 2022. "The mnemosyne number and the rheology of remembrance". *Journal of Rheology*, Vol. 66, No. 5, p. 1027–1039.

Kisler, S.F. and Schweizer, P.M., 1997. "Coating science and technology: An overview". In S.F. Kistler and P.M. Schweizer, eds., *Liquid Film Coating: Scientific principles and their technological implications*, Springer Netherlands, Dordrecht, chapter 1, pp. 137–183.

Link, F.B., Frey, S., Thompson, R.L., Naccache, M.F. and de Souza Mendes, P.R., 2015. "Plane flow of thixotropic elasto-viscoplastic materials through a 1:4 sudden expansion". *Journal of Non-Newtonian Fluid Mechanics*, Vol. 220, pp. 162–174. Viscoplastic fluids: From theory to application 2013.

Mewis, J. and Wagner, N.J., 2009. "Thixotropy". *Advances in Colloid and Interface Science*, Vol. 147-148, pp. 214–227. ISSN 0001-8686. Colloids, polymers and surfactants.Special Issue in honour of Brian Vincent.

Mours, H. and Winter, H., 1994. "Time-resolved rheometry". *Rheological Acta*, Vol. 33, No. 5, pp. 385–397.

Mueller, S., Llewellin, E.W. and Mader, H.M., 2010. "The rheology of suspensions of solid particles". *Proceedings of the Royal Society A: Mathematical, Physical and Engineering Sciences*, Vol. 466, No. 2116, pp. 1201–1228.

Rebouças, R., Siqueira, I. and Carvalho, M., 2018. "Slot coating flow of particle suspensions: Particle migration in shear sensitive liquids". *Journal of Non-Newtonian Fluid Mechanics*, Vol. 258, pp. 22–31.

Siqueira, I.R. and Carvalho, M.S., 2019. "A computational study of the effect of particle migration on the low-flow limit in slot coating of particle suspensions". *Journal of Coatings Technology and Research*, pp. 1–10.

Tsuda, T., 2010. "Coating flows of power-law non-newtonian fluids in slot coating". *Journal of the Society of Rheology, Japan*, Vol. 38, No. 4-5, pp. 223–230.

Valdez, L.D., 2013. *Slot Coating of Particle Suspensions*. Master's thesis, Pontificia Universidade Catolica do Rio de Janeiro, Rio de Janeiro, Brasil.

Yoon, J., Kim, D., Lee, S.H., Kang, D. and Nam, J., 2022. "Simplified model for operability window of slot coating without vacuum". *Chemical Engineering Science*, Vol. 259, p. 117766.

7. RESPONSIBILITY NOTICE

The authors are solely responsible for the printed material included in this paper.